Application of sensor technologies for local and distributed structural health monitoring

C. Sbarufatti*,†, A. Manes and M. Giglio

Politecnico di Milano, Dipartimento di Meccanica, Via La Masa 1, 20156 Milano, Italy

1. INTRODUCTION

Structural health monitoring (SHM) is intended as a diagnostic unit, able to recognize the presence of an anomaly and to characterize the damage by means of a properly designed signal processing algorithm. The goal of SHM is to improve the safety and reliability of structures by detecting damage before it reaches a critical state. It can be applied to different industrial fields and aeronautic structures. The latter, in particular, can receive benefits from an SHM application because of the large amount of required maintenance. SHM technology is being developed in view of a replacement of visual inspection and scheduled maintenance procedures with automated damage assessment processes, thus allowing a move towards condition-based maintenance. Nevertheless, damage criticality cannot be defined in general terms, e.g. assuming a general threshold target crack length that has to be detected if fatigue damage is concerned, as it strongly depends on the structure's and damage's geometries and boundary loads [1]. Many non-destructive testing methods are currently available, and direct visual inspection, liquid penetrant, eddy current, radiography, ultrasound, acoustic emission, etc. are just few of them [2]. They are used offline during maintenance and require one or more operators

*Correspondence to: C. Sbarufatti Ph.D., Dipartimento di Meccanica, Politecnico di Milano, Via La Masa 1, 20156 Milano, Italy.
†E-mail: claudio.sbarufatti@mail.polimi.it

depending on the structure complexity and dimension. One is expected to detect defects at an early stage to guarantee acceptable safety levels until the next scheduled maintenance. In practice, designers have to guarantee slow crack propagation or fail safe configurations for the entire inspection interval, however dependent on the 'degree of inspectability' of the considered structure.

In contrast, an SHM system is designed to be permanently installed and to perform continuous real-time monitoring of the structure. This would firstly result in a relaxation of the target defect dimension that has to be detected, however always depending on the considered structure and damage geometries and load configuration. Secondly, continuous monitoring can reduce inspections and idle time, thus the increase of the structure availability and duration will be a collateral consequence. Though autonomous SHM systems are far from being comparable with currently adopted non-destructive testing (unless the precise position of the damage is known 'a priori') in terms of minimum detectable crack length, design limits might be relaxed for some applications because of the possibility to classify any damage as 'in flight evident' [3] after the installation of a real-time SHM system.

Helicopters, in particular, are aircrafts that are subjected to very demanding operating conditions with regards to the fatigue loads, as a consequence of the low frequency loads associated to manoeuvres and the high frequency dynamic loading induced by the aerodynamic field of the rotor blades. Their spectra are characterized by a high number of load cycles per flight, much more than in a fixed-wing aircraft. Nevertheless, when the helicopter fuselage is concerned, the absence of cabin pressure is a strong advantage with respect to a fixed-wing aircraft, in terms of fatigue design. The specification guide for aircraft fuselage [3] states that damage tolerance should be respected for two panels (bays) of cracked skin plus the broken central stringer (or frame) for a structure that is classified as fail safe crack arrest, such as conventional skin-stringer (or frame) construction.

Three elements play a significant role in the deployment of a diagnostic SHM system: (i) the sensor network, intended as the sensor technology, the data acquisition system and the design procedure for sensor numbering and positioning; (ii) the signal processing algorithm, comprehending data fusion, feature extraction and statistical modelling for feature classification; and (iii) the experience, necessary to fuse and to interpret the enormous amount of data acquired through a sensor network, including (but not limited to) the knowledge of the operative conditions to build a statistical model of normal condition data (sufficient in case of unsupervised learning) as well as the availability of training data from structures with all conceivable damage locations and severities for example (requirement for supervised learning). Focusing on 'the experience', high-fidelity numerical models could yield considerable improvements to the SHM design optimization, as will be later explained. Numerical experience, based here on finite element models (FEMs), can be used at different design levels, from the identification of the critical regions inside the monitored structure, to the preliminary appreciation of any feature sensitivity to damage, as is explained in Section 7 of this paper, relatively to strain gauge (SG) technology. High-fidelity numerical simulations of a validated model can also be used for sensor placement and sensor density definition, as described in [4], as well as to estimate the performances of the entire diagnostic system in terms of minimum detectable crack length [5]. It is however important to consider that the ability to convert sensor data into structural health information is directly related to the coupling of the sensor system hardware development with the data interrogation procedures [6] and, hence, the software. All the elements described previously must be optimized in a coupled manner to provide an efficient SHM system.

The focus lies here on the sensor technology. Several sensor systems have been experimentally used to monitor fatigue crack growth on a series of fuselage panels (thin-walled metallic skin with riveted stringers construction) representative of the rear fuselage of a medium weight helicopter: (i) electrical crack gauges (ECGs); (ii) comparative vacuum monitoring (CVM); (iii) optical fibre Bragg grating (FBG) SGs; (iv) electrical resistance-based SGs; and (v) a Piezoelectric Smart Layer (SL). This paper is part of a wider activity aimed to fatigue crack diagnosis on helicopter fuselages. It summarizes and compares the experimental results gained with these sensor technologies on a thin-walled metallic structure. The attention is focused on the evaluation of the sensor suitability for SHM strategies, considering practical installation requirements and damage sensitivity. The influence of varying operative load condition is also taken into consideration, especially for FBG and SL sensor networks. When making such a comparison, it should be noted that the authors do not believe there is one sensor that is optimal for all SHM problems. All of these sensors have relative advantages and disadvantages, which have been pointed out during fatigue tests on a typical aeronautical structure. Also, the technologies described are not at the same level of maturity for SHM application and, hence, some may require more development, while others are readily available with commercial solutions.

The layout of the paper is as follows: the specimen under monitoring and the two considered damage configurations are shown in Section 2; a brief introduction to the selected sensor technologies is provided in Section 3, in which sensors for local and distributed monitoring are classified. The experimental activity is detailed in Section 4, including the test programme, the sensor and the hardware configurations. Damage sensitivity and suitability for on-board monitoring have been discussed in Sections 5–8, for ECG, CVM, SG and a piezoelectric SL, respectively.

Focusing on Section 7, experimental data acquired from an FBG sensor network have been compared with numerical data obtained from a FEM, proposed as reference for SHM design. A comparison of electrical strain gauges with optical FBG technology is also carried out.

Particular attention is drawn within the paper to the description of damage versus load sensitivities. The uncertainty in some selected features due to the variation of the operative conditions (load in particular) is investigated in Sections 7 and 8 for the FBG and SL sensor network technologies, respectively.

A conclusive section is finally provided in Section 9.

2. SPECIMEN AND DAMAGE CONFIGURATION

2.1. The specimen

The rear fuselage of a helicopter has been selected as the best candidate for the application and testing of some sensor technologies for SHM. It is a highly loaded structure, with stresses coming from the reaction to the torque induced by the main and tail rotors and is designed according to a damage tolerant approach; it consists of a typical aeronautical semi-monocoque structure consisting of a skin stiffened with frames and stringers connected by rivets. Furthermore, it is a part that is difficult to access internally but is externally accessible for visual or conventional inspection. Nevertheless, some structure simplification was required to allow a complete test programme, as described in Section 4.1, with a certain number of test repetitions.

In practice, the real structure can be well represented in its damage tolerant behaviour by a stiffened panel (Figure 1), composed of a skin plus some stiffeners (stringers), connected by means of riveted joints. On one side, these joints give the structure an optimized and eventual redundant load path in case damage is present on the skin; on the other side, riveted joints often act as nucleation points for the cracks. Thus, it has been decided to test and demonstrate the activities on some stiffened straight panels (the real fuselage curvature was eliminated), designed according to the typical aeronautical practice. The main advantage is the possibility to repeat the damage propagation test on many specimens, thus also appreciating the extent of the damage sensitivity uncertainty. This would be impractical in

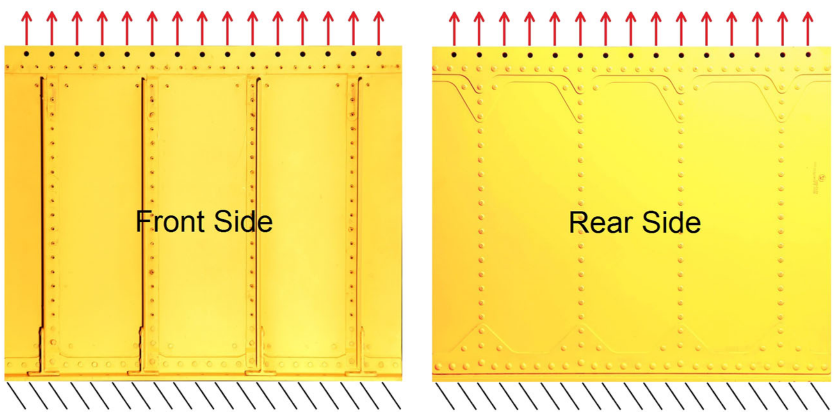

Figure 1. Specimen representative of a helicopter rear fuselage panel; load is applied vertically at the upper edge, while the panel is grounded at its lower edge.

case of complex geometries, but it is absolutely necessary for a preliminary activity, aimed to appreciate the suitability of different sensor technologies for SHM applications.

The three-bay panel consists of a 500×600 mm skin, stiffened through four riveted stringers. The thicknesses of the skin and stringers are 0.81 and 1 mm, respectively. Twenty equally spaced (21.5 mm) rivets connect each stringer to the skin. Skin and stringers are made of Al2024-T6 and Al7475-T76, respectively. The lower edge of the panel presents a link for the connection to the ground, which simulates the skin-stringer-frame link of real structures. The upper edge of the skin is reinforced through thickness elements to allow for load application and distribution. Four butt-straps are also used to transfer the load from the skin to the stringers.

2.2. Damage configuration

Two types of damage have been artificially induced on different panels and then propagated under fatigue load to evaluate damage-related feature sensitivity differences with various sensor technologies:

- Case 1: crack on the skin, positioned in the centre of the panel bay (Figure 2(a)).
- Case 2: crack on the skin, starting from a rivet after stringer failure in correspondence of the same rivet. (Figure 2(b))

Case 1 (hereafter referred to as *skin crack* damage) is representative of a crack generated after impact damage in a generic location of the panel skin. It can be demonstrated that a combination of shear and tensile stresses over the skin might induce stress concentration also in some bay areas, thus potentially increasing the crack growth rate.

Case 2 (hereafter referred to as *stringer failure* damage) has been selected to consider the worst case of damage, which should correspond to the maximum crack propagation rate. As a matter of fact, it is a damage configuration that is usually adopted to verify damage tolerance of aeronautical structures [3].

3. SENSOR CLASSIFICATION AND SELECTION

Two classes of sensors can be used for on-board structural diagnosis: either local sensors can monitor regions were cracks already exist or where they are most likely to form; or distributed sensing is applied, which involves a smart network of sensors providing a large amount of data, to be fused and interpreted through a database of experience (either virtual or experimental) for diagnostic and prognostic purposes. Both types have been tested in the framework of the current research and a brief presentation of the selected technologies is reported in this section. A summary of the characteristics of each sensor technology is given in Table I. References are provided for each sensor, which give a more detailed explanation of the working principles.

3.1. Local sensors

Local sensors are suitable if precise regions where a crack appears are identifiable either through a service database or by means of a numerical model (e.g. a FEM) in order to estimate a priori the most critical regions inside the airframe, thus locating a restrict number of sensors in the hot spots.

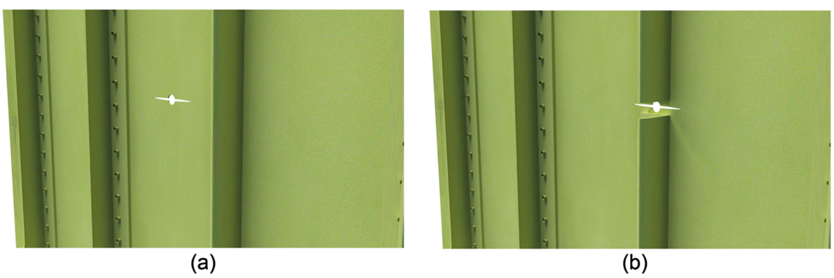

Figure 2. (a) Skin crack artificially induced in the centre of a bay, and (b) skin crack propagated from a rivet hole after induced stringer failure.

Table I. Sensor classification.

Sensor ID	Sensor type	Damage measure	Signal type
ECG	Local	Direct measure	Electrical
CVM	Local	Direct indication	Pressure differential
Electrical resistance-based SG	Distributed	Feature extraction	Electrical
FBG	Distributed	Feature extraction	Optical
SL	Distributed	Feature extraction	Electrical

ECG, electrical crack gauges; CVM, comparative vacuum monitoring; SG, strain gauge; FBG, fibre Bragg grating; SL, Smart Layer.

Crack gauges are a typical example of a local sensor. In particular, *ECGs* [7] are a mature technology which are nowadays used for structure monitoring of fatigue crack damage. They consist of a circuit of many parallel wires that break when the crack passes through them, thus provoking a step change in the total electrical circuit impedance (Figure 3).

Comparative vacuum monitoring sensors [8–10] are non-electrical crack gauges, consisting of a depressurized circuit (Figure 4). Void is induced on the circuit channels, and the monitored structure represents one side of the channel. The passage of a crack will generate a measurable air flow, which is an index of the crack presence. CVM sensors were first installed on a US Navy H-53 helicopter in 2002 as part of a trial programme. The sensors were installed in front of an existing crack in a location that required approximately 4 h to disassemble, inspect and reassemble. This inspection was required every 25 flight hours on a large and heavily used fleet, but was reduced to approximately 5 min with the CVM system without any requirement to disassemble the aircraft.

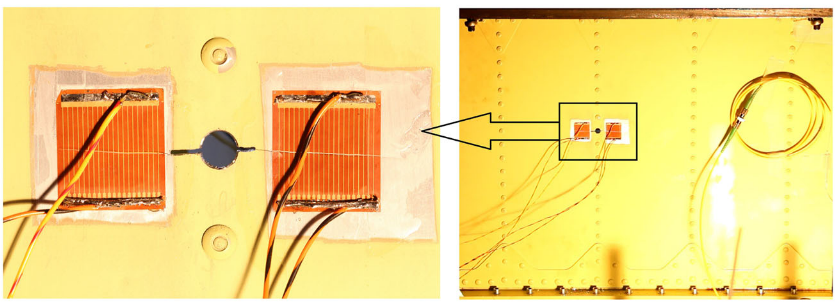

Figure 3. Electrical crack gauge sensor. The passage of a crack results in multiple wire breakage, thus modifying the total circuit impedance.

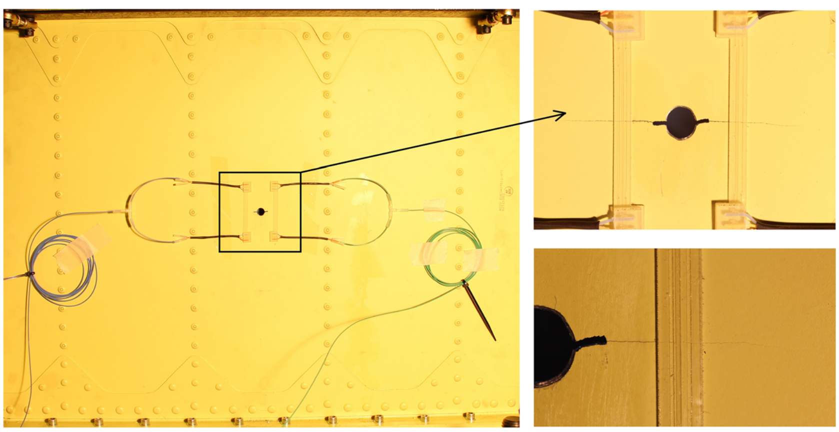

Figure 4. Comparative vacuum monitoring sensor. Void is induced in the sensor channels, and the passage of a crack provokes a measurable air flow.

The change induced by the crack presence in the electrical impedance (ECG) and pressure (CVM) can be monitored by 'ad hoc' devices that show discontinuity in the acquired signal, as expressed in detail in Section 4.3, thus guaranteeing a direct indication of damage existence.

3.2. Distributed sensor network

If a large structure with many possible crack nucleation regions has to be monitored, a distributed sensor network will have to be designed to be permanently installed on the monitored region providing indication on the damage existence as well as to infer the characteristics of that damage. One has to identify the most suitable damage sensitive feature (as illustrated in the following) upon which to perform the whole inference and contextually to select the most apt technology to sense it. A fundamental premise regarding distributed sensing is that these systems do not directly measure damage. They measure the response of a system to the load condition in the operational environment (as for the case of FBG SGs) or the response to active inputs generated within the sensor network (as for the case of a piezoelectric SL). Depending on the adopted sensing technology and the type of damage to be investigated, the sensor readings may be more or less directly correlated to the presence, type, location and dimension of the damage. The two primary steps for the success of the SHM system are the selection of a damage sensitive feature as well as the definition of a statistical model to classify the same feature [6].

The possibility to perform feature extraction based on a numerical experience rather than experimentally is particularly attractive, as anticipated in the introduction. However, the literature reports limited success in developing diagnostic systems trained on simulated data that can generalize well to the real situation, and available references have been provided throughout this section. Focusing on feature extraction, three main classes can be defined, comprehending those features mostly adopted in the literature.

Dynamic features include natural frequencies, mode-shapes, modal strain energy, frequency response functions, etc. Extensive data have been published on vibration-based monitoring systems [11–13]. Micro Electro-Mechanical Systems technology appears to be very promising within this context [14]. SGs are also often used for these purposes. These methods are widely adopted in both civil and aerospace engineering for structure monitoring, sometimes involving the usage of numerical models (FEM) and machine learning algorithms (artificial neural networks (ANNs)) as a statistical model for feature classification, as reported in [15]. A vibration-based damage diagnosis based on mode shape analysis was presented in [16], where quantification and localization of damage were performed on a simple beam-like structure, combining FEM with ANNs and also providing an experimental validation.

Static features include the acquisition of a static field (e.g. strain field) at some predefined locations over the monitored structure, then processing the acquired feature pattern in a post-processing algorithm to highlight the presence of an anomaly and to make inference over the damage characteristics. Focussing on the use case presented in this paper, the helicopter fuselage is subjected to a wide range of low frequency loads (due to helicopter manoeuvres) that have predominant amplitudes with respect to high frequency loads. As manoeuvres induce static loads on the airframe, it is possible to interpret the induced strain field as a static variable, neglecting the dynamic component. SGs are obviously the most apt technology if the strain field sensitivity to damage is investigated. The possibility to accurately model the strain pattern and consequently the static and fatigue behaviour of a stiffened structure with finite elements has been demonstrated in [17,18]. FEMs combined with ANNs have been successfully used in [19] to diagnose multiple site damage in riveted structures, based upon the simulated knowledge on the strain field, however without a validation test on the real structures, thus proving that the strain field sensitivity to crack damage can be exploited for SHM.

Mechanical guided waves scattering (Lamb waves primarily) is also a widely investigated source for damage identification [20–23], based on a network of piezoelectric sensors and actuators (Figure 5(b)) able to sense the scatter of waves travelling across a medium, induced by the presence of damage in a certain location and with a given dimension. The monitoring principle of guided ultrasonic waves is similar to the acoustic-ultrasonic technology. However, guided waves utilize well-defined modes and paths of propagation [24,25]. Lamb waves have the advantage that they can travel long distances in metallic structures and therefore allow interrogation over a large area. In general terms, the presence of damage along the

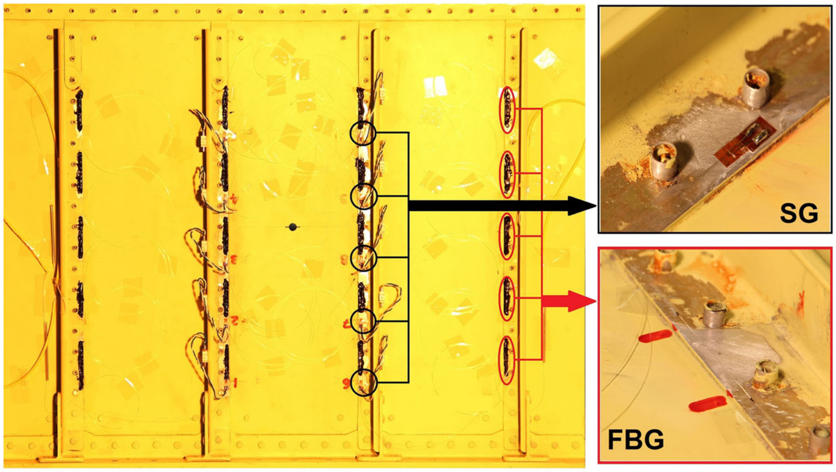

(a)

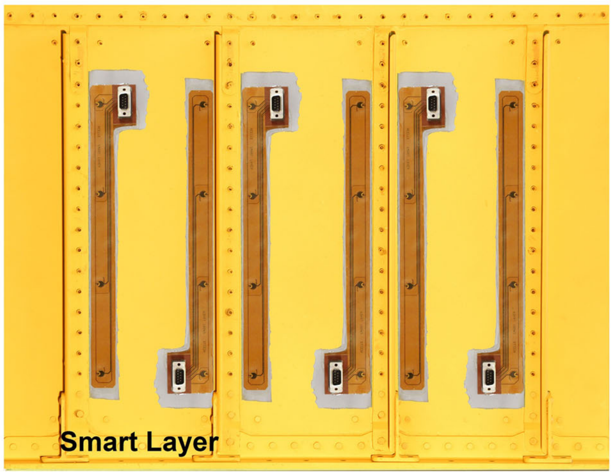

(b)

Figure 5. Distributed sensor networks. (a) 20 fibre Bragg grating (FBG) sensors located on the stringers under the black glue, and 10 strain gauges (SGs) positioned on the two central stringers. (b) Smart Layer comprehending 24 piezoelectric transducers for Lamb wave signal actuation and sensing.

travelled distance induces a delay in the received signal as well as a modification in the signal peak amplitude, which can be exploited for damage identification. A remarkable work is reported in [26,27], where the authors tested a model-based diagnostic system based on Lamb wave scattering for the quantitative diagnosis of through-hole-type defect in a CF–EP quasi-isotropic laminate. A similar approach is used in [28] to provide indication on crack damage position and dimension over an aluminium skin, taking advantage of supervised machine learning algorithms trained on a numerical experience and capable to generalize in a real experimental condition.

As far as sensors types are concerned, *FBGs* have been selected from the available technologies for strain sensing (Figure 5(a)). FBGs are grid-like patterns, inscribed into an optical fibre core. The possibility to multiplex a certain number of FBGs within a single optical fibre (the allowed number is strictly dependent on the maximum strain to be measured) is particularly attractive for smart sensor network design. This technology allows the reduction of the logistic impact due to the installation of many sensors for large area scanning. They are non-electrical sensors and offer several advantages including light weight, low power consumption, immunity to electromagnetic interference (EMI), long lifetime and high sensitivity. Furthermore, they require no initial and in-service calibrations and are affected by a very low signal drop. All these advantages contribute to make FBGs (as well as the piezoelectric transducers presented later) one of the most attractive technology for SHM purposes. Some success has been attained in developing smart systems capable to diagnose fatigue damage in metallic fuselage structures like the one tested hereafter [5]. Research on fibre optic monitoring systems is still very active, especially concerning the health condition assessment for composite materials. A valid example is represented by the SARISTU project [29] (*Smart Intelligent Aircraft Structures*), funded by the European Seventh Framework Programme, in which a part of the work is devoted to the integration of a fibre optic-based monitoring system on a generic wing and fuselage composite structure, aiming to implement the system during the composite manufacturing procedure, then monitoring the assemblies' status throughout their entire life. Some practical information regarding the utilization of FBG sensors for fuselage crack monitoring is reported in Section 7, where a comparison with the consolidated *electrical resistance-based SGs* is also performed (Figure 5(a)). Nevertheless, strain field sensitivity to boundary load condition is the main drawback. Absolute strain is much more sensitive to the applied load with respect to any damage of acceptable size. Particular attention has to be paid to extract a damage sensitive feature.

An active piezoelectric sensor network (Figure 5(b)) has also been tested, and some practical considerations regarding its suitability for crack detection on a typical helicopter fuselage are reported in Section 8. Travelling waves (Lamb waves for the particular case under examination) are less sensitive than any strain field measure to the applied load configuration. Proper feature extraction is however required and often difficult to obtain, because of the influence of complex wave reflections at any structural boundary. Furthermore, each transducer inside the network requires its own cabling circuit to receive power and transfer signal; the *SL* layout proposed by Acellent Technologies [30] has been adopted here and appears to represent a feasible solution for practical applications.

4. EXPERIMENTAL TEST CONFIGURATION

4.1. Experimental test programme

Seven fatigue crack propagation tests have been carried out on seven panels like the one shown in Figure 1. Different sensor configurations have been adopted for each test, involving the usage of local and distributed sensor technologies, as listed in Table II.

Initial data have been acquired on the undamaged panel. Damage has then been artificially induced: a 16-mm wide notch (Figure 2(a)) was introduced to initiate skin crack damage, as calculated to obtain a stress intensity factor compatible with crack propagation (in relation to the applied load condition described in the succeeding text). Concerning stringer failure, the stringer was artificially cut in correspondence of a rivet and a crack was initiated from the same rivet hole (Figure 2(b)).

Following the damage initialization, a sinusoidal 12 Hz load has been applied vertically to propagate a real crack over the panel specimen, and the acquisition system has been activated, as described in detail in the succeeding text. The maximum load amplitude has been set to 35 kN with a load ratio $R = 0.1$. A single frequency load spectrum with constant amplitude is evidently far from a realistic scenario, especially for helicopter applications. The load spectra applied during structural certification are composed of different spectra and simulate different manoeuvres like ascending, turning, descending, etc. [31]. However, such a single load spectra is a necessary step for the preliminary evaluation of the

Table II. Description of the fatigue crack propagation test programme with an indication of the type and number of sensors installed on each specimen.

Test	Damage	ECG	CVM	Electrical resistance-basedSG	FBG	SL
1	Skin crack			x10	x20	
2	Skin crack				x20	
3	Skin crack				x20	
4	Skin crack	*x*2			x20	
5	Stringer failure	*x*2		x5	x20	
6	Skin crack		*x*2			x24
7	Stringer failure		*x*2			x24

ECG, electrical crack gauges; CVM, comparative vacuum monitoring; SG, strain gauge; FBG, fibre Bragg grating; SL, Smart Layer.

sensor system performances, which allows the reduction of the load uncertainties and the focus on damage sensitive features (for distributed sensor networks). In particular, the considered load level is typical for the characterization of a helicopter structure under manoeuvre, approximately at high-medium loading level [31].

The length of the crack has been recorded during the experiment by means of mechanical measurements (calliper).

4.2. Sensor configuration

Local sensor positioning must be based upon previous results on real similar structures or on numerical calculations of stress distribution over the monitored specimen, to locate the sensors in the exact position where a crack will nucleate. Furthermore, if a crack already exists but it is judged as non-critical, the structure may be left in operation, though with a local sensor installed to monitor crack propagation. The latter is the approach undertaken in the present research. In practice, cracks are artificially induced and local sensors are thus positioned to assure the interception of the propagating damage, as shown in Figures 3 and 4 for the ECG and CVM, respectively. In particular, two ECGs have been installed for tests 4 and 5, while two CVMs intercept sensors are used in tests 6 and 7, to monitor both tips of the propagating damage.

Distributed sensor network design is a very active research field and consists of the definition of techniques to optimize the sensor number and position to reach the optimal configuration as a compromise between the installation costs and the increase of some reliability parameters. Sensor network optimization is outside the scope of the present paper. Nevertheless, concerning the FBG network layout, sensors have been placed on the stringers due to the fact that they produce signals that are affected by less uncertainty than sensors on the skin [4]; this is particularly advantageous if one has to classify any structural condition based on a simulated test set up, which requires a strong correlation of experimental and numerical data. Furthermore, the sensor number has been optimized as described by the same authors in [32], resulting in the FBG network layout shown in Figure 5(a). As is shown in Section 7, FBG measures are compared with the electrical resistance-based SGs for tests 1 and 5. In particular, the SG layout for test 1 is indicated in Figure 5(a), where 10 SGs have been distributed on the two central stringers; only five SGs have been installed during test 5, which are located on the central-left stringer. The piezoelectric sensor network (SL) layout (Figure 5(b)) has been designed according with the sensor system manufacturer experience [30] to obtain sufficient feature sensitivity to identify the two damage types presented in Section 2.2.

4.3. Hardware configuration

Electrical crack propagation gauges HBM-RDS20 provide a step signal that can be acquired with an SG amplifier (NI-SCXI), upon the addition of an interface circuit [7] necessary to limit the unbalance of the measuring bridge (Wheatstone Bridge) within acceptable limits, imposed by the saturation of the acquisition instrumentation. Two sensors have been simultaneously acquired in two separate channels, and data have been saved on a desktop PC in real-time during crack propagation.

The hardware apparatus for CVM sensing requires the utilization of a vacuum source (KVAC), which supplies a constant vacuum of 20 kPa below ambient air pressure. Each CVM sensor is etween the vacuum source and the sensor system, dependent on the air flow through the sensor induced by the passage of a crack. Data from two sensors has been simultaneously saved on a desktop PC running SIM Utility software provided by the hardware and sensor manufacturer (Structural Monitoring Systems Ltd, Nedlands, Australia) [8].

The simultaneous acquisition from the 20 FBG sensors has been performed with the four-channel optical interrogator HBM-DI410. The sensor is an HBM OptiMet-OMF optical fibre. Five FBGs have been multiplexed on each single optical fibre and are simultaneously read by one of the four interrogator channels. A maximum 1 kHz sampling rate can be achieved for each FBG sensor. Each sensor signal is then transferred to a desktop PC. HBM-Catman Easy-AP software (HBM, Darmstadt, Germany) has been used as an interface between the desktop PC and the optical interrogator.

Electrical SG signals have been acquired with NI-SCXI amplifier module, with a sampling rate of 1 kHz. To ensure accurate measurement results, Shunt calibration has been separately performed to each SG sensor, thus calculating a scaling factor for each SG, accounting for any signal bias induced by the signal conditioning apparatus, including cables. Data have been saved on a desktop PC.

The diagnostic hardware-software platform made by Acellent [30] has been used for the SL signal processing. As anticipated in the preceding text, SL provides an active SHM, where each piezoelectric transducer acts both as an actuator and as a sensor. Lamb waves were launched by driving the actuator with a five cycle tone-burst at 150 kHz frequency, modulated with a Hanning window. The Lamb wave signal induced through one piezoelectric transducer travels across the monitored medium and is acquired by one neighbour sensor. A total number of 136 paths have been designed to cover the entire monitored area, as indicated in Figure 6(a). Each path is sequentially scanned to verify the consistency with a baseline undamaged preliminary acquisition. *ScanGenie* (Acellent Technologies inc., Sunnyvale, CA, USA) has been used as waveform generator and signal acquisition system. A multiplexer switch amplifier box is interposed between the ScanGenie and the transducers to select the proper actuator and sensor each time a new path is considered (path switch frequency was 1 Hz). Data have been automatically saved on a desktop PC running ACESS software (Acellent Technologies inc., Sunnyvale, CA, USA), where a preliminary data visualization and analysis is performed in real-time (Figure 6(b)).

5. ELECTRICAL CRACK GAUGES

5.1. Sensitivity to damage

The step curves generated with the ECG sensor located as in Figure 3 during tests 4 and 5 are shown in Figure 7. In particular, the average value of the signal acquired at each step of the crack propagation (each time a new grid wire is broken) has been reported in Figure 7(c). If equal parallel wires are used to build the sensor, the non-linear relationship between the change of total circuit impedance and the number of broken wires will generate a non-linear correlation between sensor output and crack length. This will provoke shorter signal steps when the first sensor grid wires are broken and larger signal discontinuities when the last links fail, thus compromising the sensor robustness for shorter cracks. Depending on the number of samples forming the average, signal discontinuities can appear more or less definite. This is due to the noise inevitably present in the signal, caused by the conditioning circuit as well as the mechanical strain induced by the dynamic boundary loads. Nevertheless the latter is strongly reduced by a factor equal to the number of parallel wires composing the sensor grid.

The extent of the sensor noise is clearly visible in Figure 7(a) and is compared with the signal step induced after the failure of the first grid wire. Assuming the signal can be treated as a Gaussian distribution (as shown in Figure 7(b)), the ratio between the standard deviation of the baseline signal and the extent of the step provoked by the first wire failure is equal to 0.53. Thus, the noise uncertainty is larger than 50% of the discontinuity amplitude.

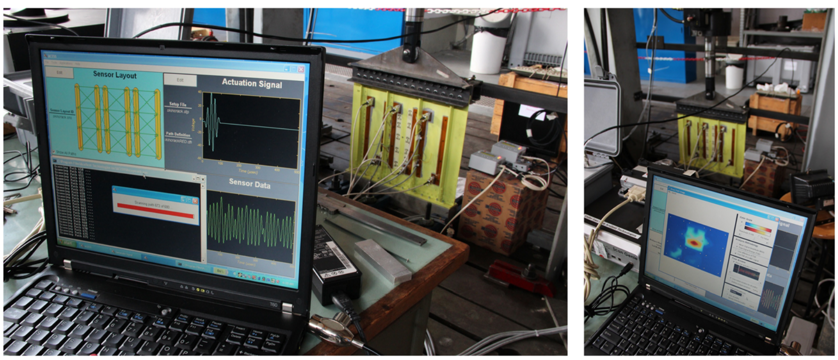

(a) (b)

Figure 6. Smart Layer utilization during test 6. (a) ACESS software has been set to automatically scan the required number of path. (b) The system provides indication on damage location based on signal comparison with baseline condition.

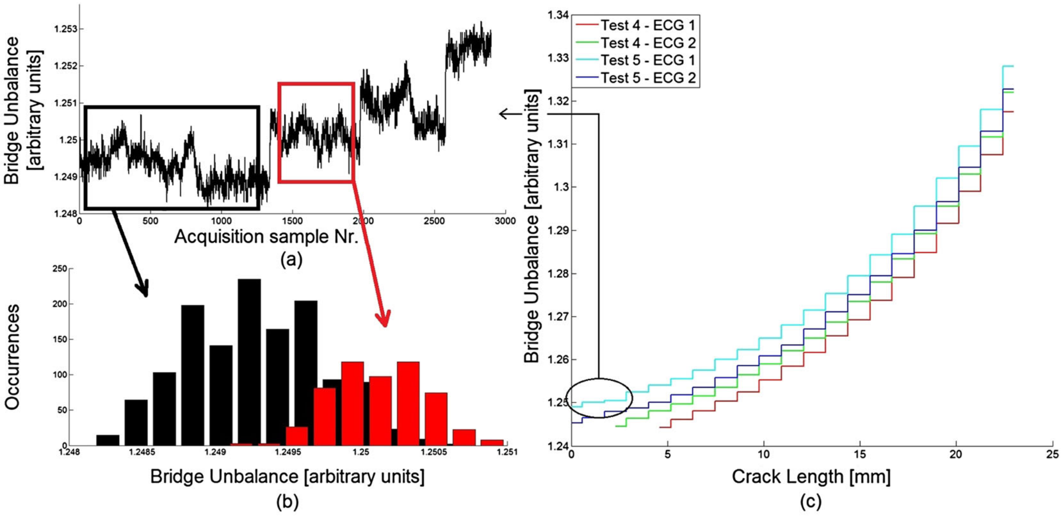

Figure 7. Four step signals provided by electrical crack gauges (ECG) sensors (c); noise is particularly effective on the first steps (a), where the standard deviation of the signal distributions reaches 53% of the discontinuity step.

The robustness of the sensor output can be increased with linear output ECGs. If a linear output is required, it is obtained in two ways: (i) using sensors with wires in parallel characterized by different lengths, correspondent to different electrical resistances (Figure 8(a)) or alternatively (ii) using sensors with wires in parallel characterized by different diameters, thus different electrical resistances. The calibration curves obtained with four linear output ECG sensors have been reported in Figure 8(b). Output linearity is obtained increasing the impedance of consecutive wires belonging to the sensor grid, as shown in Figure 8(a). Differently from the case reported in Figure 7, the signal has not been continuously acquired but is acquired at some predefined steps during crack propagation. Two consecutive output points have been connected with a straight line to highlight output linearity.

5.2. Suitability for on-board monitoring

The sensor requires the removal of protective coatings and a thorough surface cleaning to be perfectly adherent to the monitored structure. This represents a problem especially for helicopter applications, as the structure is often exposed to very harsh environments, where corrosion is a major issue.

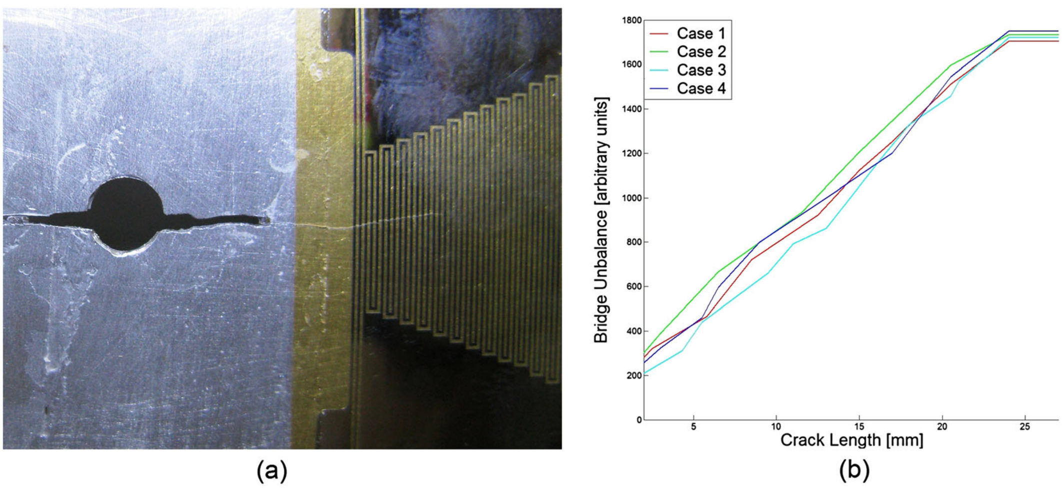

Figure 8. (a) Example of electrical crack gauges sensor designed to provide a linear output curve, as indicated in (b) where the calibration curves for four sensors have been presented.

The sensor consists of an electrical circuit, and it is not recommended for critical environments in presence of inflammable or explosive materials. Furthermore, this technology is not immune to EMI. Particular care has also to be taken to avoid short circuits when the sensor is bonded to metallic structures.

Electrical crack gauges have a relatively large damage sensitivity; nevertheless, they are local sensors and must be placed along the crack path to provide useful information. However, the adoption of linear output sensors is recommended to increase the sensitivity to shorter damages, when strictly necessary, as non-linear sensor output sensitivity is poor and less robust during the first crack propagation steps.

If a real-time on-board monitoring of any existing crack has to be performed, a signal processing methodology for the robust identification of signal discontinuities has to be adopted, especially if non-linear output sensors are adopted. The sensor can provide indication of damage existence and crack damage quantification, though in a small propagation range (up to 20 mm).

6. COMPARATIVE VACUUM MONITORING

6.1. Sensitivity to damage

The experimental results conducted on an aluminium stiffened skin structure are reported in Figure 9. CVM acquisition has been conducted in real-time during crack propagation, while a sinusoidal fatigue load (load ratio R = 0.1, peak load 35 kN) has been applied to the structure.

Once the sensor circuits are connected to the reference vacuum source (KVAC) via a flow metre (SIM), sensor channels are maintained at 20 kPa below ambient pressure. The SIM measures the pressure differential between the KVAC and the sensor channels, thus providing the CVM output. Even when no crack is present, a certain air flow can be measured, as clearly shown in Figure 9(a) relatively to one selected sensor during test 6 and before the arrival of any crack. The pressure differential measured with no crack is an index of the permeability of all the materials defining the sensing system [33]. Some spikes are also clearly evident, due to the activation of the vacuum pump inside the KVAC,

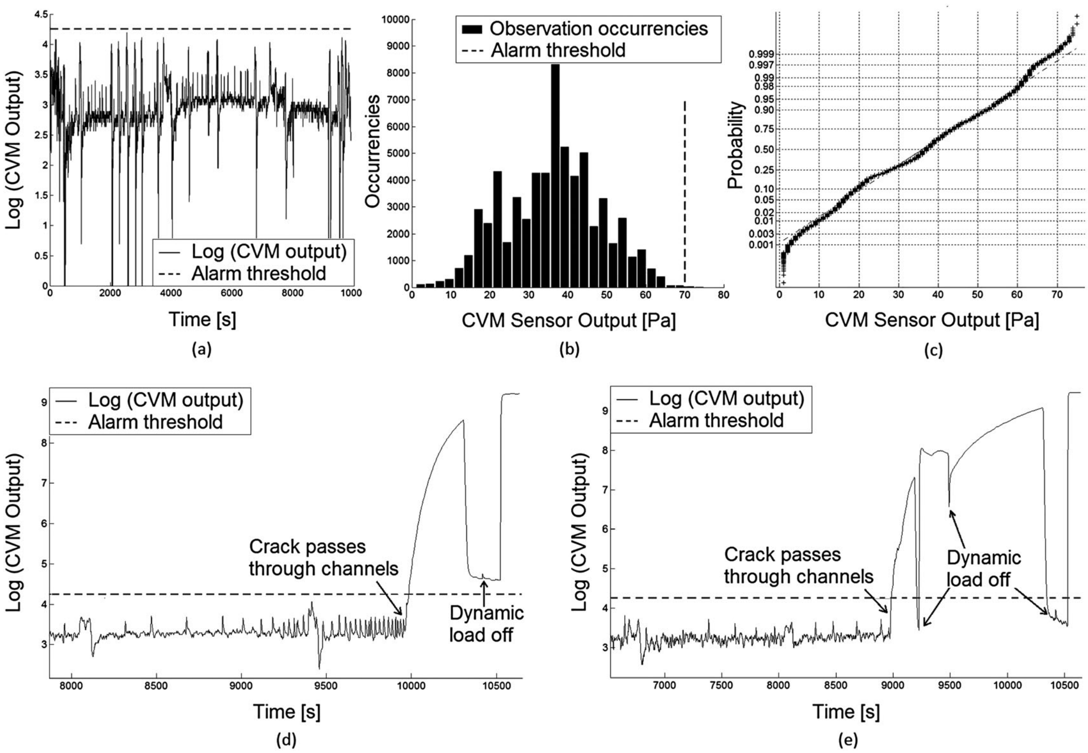

Figure 9. Analysis of the comparative vacuum monitoring (CVM) signal; (a) baseline signal from a CVM sensor installed during test 6; (b) approximation of the baseline signal distribution through histograms with an indication of the 99.9% confidence threshold; (c) normal probability plot of the distribution in (b); the CVM output signal is shown in (d) and (e), as acquired from the two sensors installed during the fatigue crack propagation test 6.

necessary to maintain the reference vacuum chamber at the desired depressurization level. The manufacturer specifies that the acceptable range of readings lies between 0 and 150 Pa if no crack is present. The range is, however, dependent on the size of sensors and the length of tubing system. Figure 9(b) represents the CVM sensor output distribution when no crack is present and has been obtained collecting the four baseline signals from the CVM sensors used in tests 6 and 7. The normal probability plot in Figure 9(c) demonstrates that such a distribution can be assumed to be Gaussian. The 99.9% confidence threshold (corresponding to indicatively 70 Pa) has been reported in Figure 9(b) and has been used as a term of comparison to raise the alarm. However, the 150 Pa value specified by the manufacturer can be used to guarantee better robustness against false alarms.

The sensitivity to the passage of a crack can be appreciated in Figure 9(d) and (e), where the time signals recorded during test 6 have been plotted in logarithmic scale. The signal immediately departs from the baseline condition when the crack compromises the sensor channel integrity and a continuous increase is recorded, while the crack passes the entire sensor. Nevertheless, one drawback has to be highlighted. In practice, if the signal is acquired on the loaded structure (a traction load is assumed here during fatigue tests), the crack is open and an evident air flow is measured. If the load is turned off, the crack will apparently close, and the air flow will reduce as a consequence. This did not provoke any misclassification of the structural condition by the sensor represented in Figure 9(d). Nevertheless, misclassifications have occurred in Figure 9(e). Obviously, the bigger the damage, the lower the possibility for misclassification after load removal. As a matter of fact, the same test has been repeated during test 7, when stringer failure has been induced, and no misclassifications have occurred.

6.2. Suitability for on-board monitoring

The sensor installation has proved to be easy and the sensor manufacturer [8] has guaranteed the possibility to operate damage monitoring with CVM without removal of the primer coating. This is an advantage with respect to electrical crack gauges, especially if one has to monitor cracks on an ageing structure.

Two fatigue tests on two fuselage panels have been executed. Two CVM sensors have been adopted for each test to monitor both tips of the propagating crack. No sensor de-bonding has been encountered after about 400 000 cycles, even after the crack passed through the sensors. Each cycle is representative of helicopter manoeuvres, thus characterized by higher amplitude with respect to the high frequency load associated to rotor vibration. The level of strain in correspondence of the sensor position and for the undamaged condition has been in the order of 700 $\mu\varepsilon$, as calculated with the FEM presented in Section 7.1. Nevertheless, the strain during the passage of the crack is expected to be much higher.

Comparative vacuum monitoring is a non-electrical sensor, thus particularly attractive for aeronautical applications due to its immunity to EMI. Moreover, it is a suitable technology for hazardous environments, due to complete absence of electrical circuits at sensor location.

Damage sensitivity is good, especially for the online real-time monitoring, as the presence of dynamic load maintains the crack open during acquisition. Misclassification has occurred for one sensor in the offline condition monitoring, due to the apparent crack closure after the removal of the load, which probably fails to induce a measurable air flow through the sensor channels. The presence of protective coating on the aluminium structure might have facilitated this phenomenon. This can be an obstacle if the system is ran during scheduled offline maintenance and represents a drawback with respect to ECG technology.

Intercept sensors have been tested in the current paper. Contrarily to ECG sensors, they are only capable to provide a warning signal based on damage existence, without any indication about crack propagation. Nevertheless, though the technology has been preliminary tested in a localized monitoring framework, CVM can be designed with any shape to monitor large regions of complex geometries, which is another advantage with respect to ECG sensors.

A comparison summary between ECG and CVM sensors is reported in Table III.

7. FIBRE BRAGG GRATING

As anticipated in the preceding text, FBGs are a suitable technology for the distributed monitoring of the strain field. Though they consist of strain gauges for the local measure of the strain field, their

Table III. Comparison between electrical crack gauges and comparative vacuum monitoring sensors.

	ECG	CVM
Signal type	Electrical	Non-electrical
Installation	Experience required	Easy
Primer removal	Required	Not required
Offline application	Affordable	Some issues due to crack closure
Online application	Affordable	Affordable
Damage Sensitivity	Moderate	High
Suitability for large areas	No	Moderate
Suitability for anomaly detection	High	High
Suitability for localization	No	No (with single circuit configuration)
Suitability for damage description	Small quantification range available	No (with single circuit configuration)
Required experience for damage description	No	No
Sensitivity to operational environment	Low	Low

ECG, electrical crack gauges; CVM, comparative vacuum monitoring.

multiplexing capability allows for the installation of multiple sensors with a reduced logistic impact, thus allowing for the realization of a distributed sensor network capable to monitor a relatively large portion of the structure (Figure 5(a)). The disposal of a validated FEM (Section 7.1) is an advantage during the SHM design procedure. It potentially provides an indication of the sensitivity level of the selected damage-dependent feature, thus allowing defining the most convenient sensor placement strategy [4] and predicting the diagnostic system performances [5]. The sensitivity to damage for some selected sensors is shown in Sections 7.2 and 7.3, where a quantification of modelling error is also provided. The influence of random load on the selected damage index is also investigated in Section 7.4 and some conclusions on FBG technology suitability for SHM are provided in Section 7.5.

7.1. Specimen finite element model

A finite element modelling strategy has been adopted here to simulate the strain field modification induced by the presence of damage in the monitored specimen. Simulated results are only used as a term of comparison with the either electrical (resistance-based) or optical (FBGs) strain gauges. A brief description of the FEM is provided in this section, though for a more detailed presentation refer to [17,18].

The FEM is developed with ABAQUS 6.9 (Dassault Systemes Simulia Corp., Providence, Rhode Island, USA) and is shown in Figure 10, in which a comparison of the strain field in the undamaged and damaged conditions has been presented. Both stringers and skin have been modelled with quadratic shell elements (S9R5), while rivets have been simulated through three-axes springs, with their shear stiffness K_s parameter defined according to Swift's formula [34], and their axial stiffness K_a calculated by treating them as a cylindrical beam ($K_a = EA/l$) where E is the Young modulus of the rivet material, A is the area of the rivet section and l is the axial length in contact with the two aluminium shells. Each stringer has been connected to the skin by means of 20 rivets. Finally, the upper and lower portions of the panel have been specially designed to connect them to the actuator and to

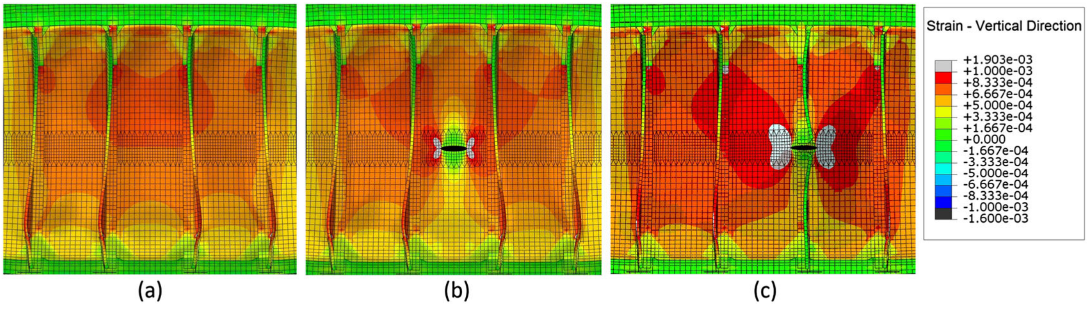

Figure 10. Comparison of the strain field distribution, measured in vertical direction (sensor direction), for (a) a healthy structure (b) a panel with skin crack damage and (c) a panel with stringer failure.

the ground, distributing the load to both the stringers and the skin, thus allowing the simulation of stress and strain in the real fuselage.

The crack damage has been simulated introducing a discontinuity in the panel skin-stringer model, by removing the links between adjacent elements along the direction perpendicular to the stringers. The same applies concerning stringer failure modelling. Because of the applied load configuration, a horizontal crack has been modelled (corresponding to crack propagation in mode I). The undamaged FEM has been verified by means of a static load test, as reported in Section 7.2. The capability of the verified FEM to predict the strain distribution in the presence of damage has been also validated in Section 7.3.

7.2. Finite element model verification in undamaged condition

The capability of the FEM to describe the strains occurring on the panel due to 35 kN static loading condition is verified in Figure 11. The undamaged panel is considered and the baseline situation (healthy structure) is verified for the five test specimens used in tests 1–5 (as indicated in Table II).

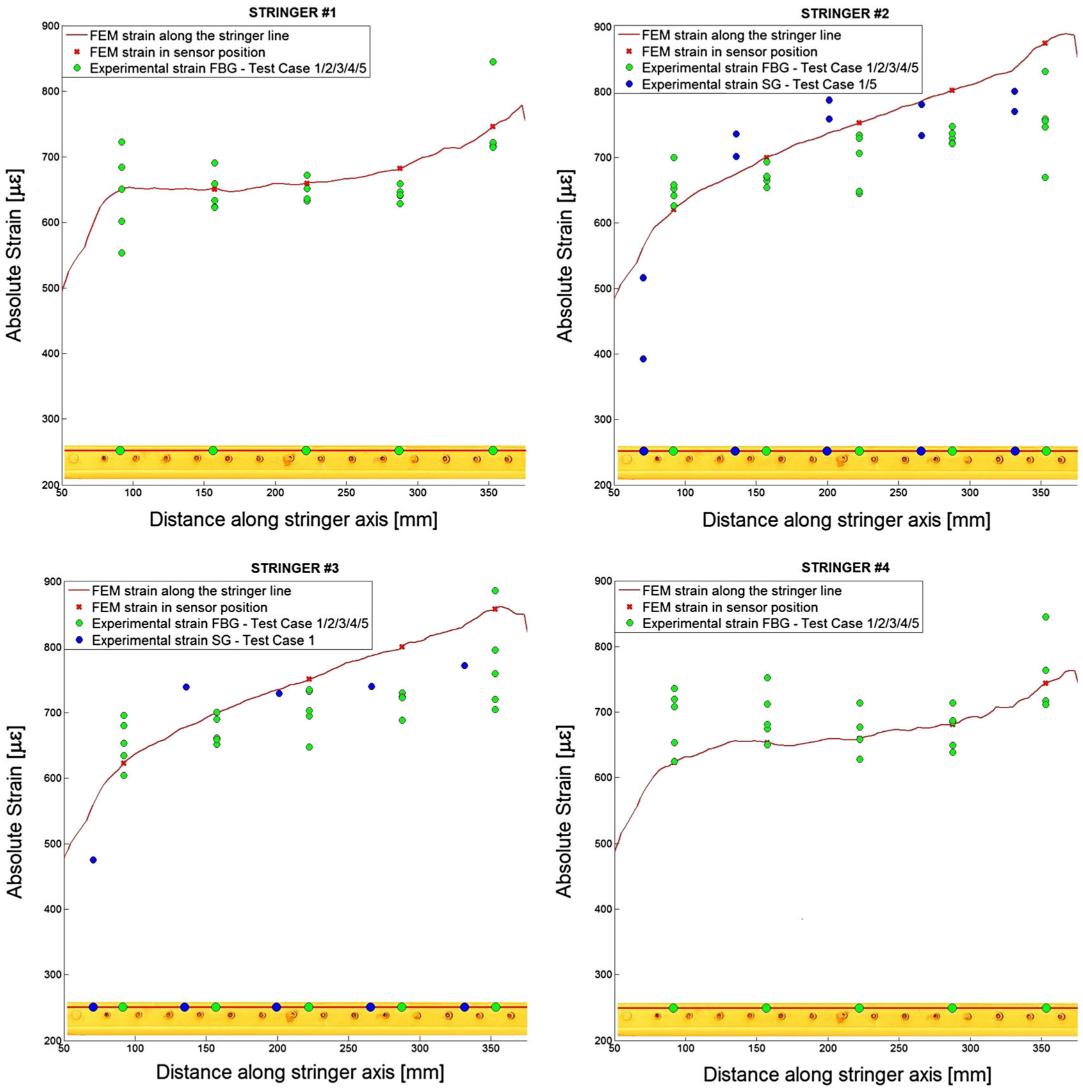

Figure 11. Comparison of numerical and experimental strains for the entire sensor network shown in Figure 5(a); stringers are labelled from the left to the right side and the undamaged configuration is considered. The distance along the stringer is taken from the panel bottom. 20 fibre Bragg grating (FBG) sensors (five sensors on each stringer) have been installed during tests 1–5. Five strain gauges (SGs) have been installed on the two central stringers during test 1 and only on stringer 2 during test 5.

The simulated FEM strains have been collected along the four stringers, and the mechanical deformations in correspondence to the virtual sensors are highlighted, to be compared with the experimental strains measured through the real FBG sensor network, distributed as in Figure 5(a).

The average error for the whole sensor network is reported in Table IV, separately for each test specimen. The error has been calculated for each sensor as the percentage difference between the strain FEM prediction and the experimental sensor measure. The error of the entire sensor network is calculated averaging the absolute value of the errors evaluated for each sensor constituting the network. The maximum sensor network error has been encountered for test 2, corresponding to 13.67%. An average error of 8.23% was encountered among the five considered specimens. This variability is due to manufacturing and assembly tolerances of the specimen and the test rig, the uncertainty in the applied load, the environmental conditions, sensor position, etc. The higher error measured for test 2 is due to the presence of a persistent bias between virtual and experimental measures. This is potentially due to a change in the environmental temperature or to a slightly different assembly configuration for the rig.

Stressing the attention on sensor positioning, some limitations arise from the technological process adopted for sensor manufacturing [35], which causes the effective position of the FBG grid to be statistically determined. The producer [36] delivers FBG chains with an indication of the area where the Bragg gratings are inscribed, however, without a precise position (Figure 12). This area is approximately 30 mm long, and the effective sensor (6 ± 1 mm long) is located within the specified limits. This is a limitation that has to be accounted for, especially if sensor signals have to be compared with a numerical model, thus requiring a precise correlation of the sensor position with their relative nodes inside the model. Furthermore, the presence of rivets causes large stress (and strain) gradients on the stringer, thus making the sensor position a crucial parameter.

Some electrical strain gauges have also been installed during tests 1 and 5. In particular, five SGs per stringer have been installed on the two central stringers during fatigue test 1, while only five

Table IV. Model validation errors, calculated with respect to the signals provided by the fibre Bragg grating network.

		Average FBG sensor network % error		
	Damage type	Undamaged – absolute strain	Damaged – absolute strain	Damaged – scaled and normalized strains
Test 1	Skin crack	6.78	7.04	1.62
Test 2	Skin crack	13.67	9.29	1.57
Test 3	Skin crack	7.29	7.19	1.57
Test 4	Skin crack	4.87	6.87	2.42
Test 5	Stringer failure	8.54	12.99	8.55
Mean		**8.23**	**8.676**	**3.146**

FBG, fibre Bragg grating.

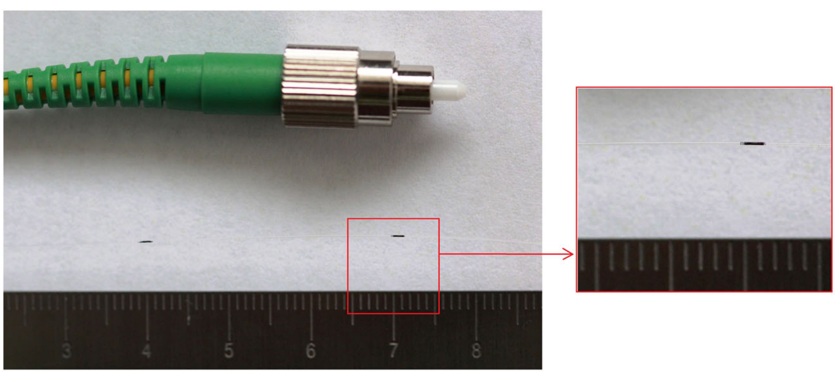

Figure 12. Bare optical fibre with connection to the interrogator channel; the fibre Bragg grating sensor position is statistically expected to lie inside the two marks provided by the producer.

SGs have been installed on the central-left stringer during test 5. Measurements in the same point with SGs and FBGs have been impractical; nevertheless, the consistency between the measures provided by the two sensor apparatus is clearly visible in Figure 11. The global average error committed by SGs (8.39%) is comparable with the one obtained with FBGs. Nevertheless, the largest contribution to the global error is provided by the two sensors that are near the lower boundary; the error is reduced to 5% if they are neglected.

7.3. Feature extraction and sensitivity to damage

Even though an error of 8% in modelling is quite a good target in general FEM utilization, variability of this magnitude is not acceptable in the current framework as it can be of the same order of magnitude as the strain field change induced by the damage itself. Furthermore, if the damage structure is concerned, the baseline error (relative to the undamaged structure) has to be summed to the error associated to the damage model. The fourth column of Table IV shows the FEM error when damage is also modelled. In particular, absolute strain data refer to the case when a 100 mm skin crack is reached as in Figures 2(a) and 10(b) during tests 1–4 and when stringer failure (with 30 mm skin crack) is induced as in Figures 2(b) and 10(c) during test 5.

Two considerations arise in order to highlight the damage-dependent feature. First, sensor network calibration on the FEM can be adapted to adjust for any *permanent bias* between the FEM and the selected specimen for the baseline condition. The procedure consists in defining a scaling factor for each sensor as the ratio between the FEM output and the real sensor measurement for the undamaged case (a separate scaling factor has to be calculated for each specimen and for each sensor). Each sensor will thus be multiplied by its scaling factor for its entire life cycle. This is impractical for some applications if FEM information has to be used to interpret real sensor signals. Nevertheless, the requirement is to perform an initial calibration of the sensors (with respect to FEM) under the hypothesis of the initially undamaged structure. Once the model biases have been eliminated, assuming that the damage modelling criteria is correct, the sensor measure should be accurately predicted by the FE model, apart from the effect of occurring non-linearity and any operative variation with respect to the baseline condition (time variable bias).

If *time variable bias* is also present, one has to resort to normalization. In practice, the effect of the boundary load has to be filtered out, while taking into consideration that the strain variation due to load is orders of magnitude higher than the damage effect over the strain field. Also the environmental temperature has an effect on the measured strain that must be compensated for. The approach used here consists in normalizing each sensor of a confined region (the entire panel might be seen as a part of the global fuselage) with respect to the average value measured by all the sensors within the same region [19]. The damage influences a small, but sufficient, percentage of the sensors and the average strain value measured by all the sensors is linearly dependent on loads and is largely unaffected by the damage. Thus, by using the average strain as a normalization factor for each single sensor, the effect of the load can be filtered out. The method remains valid only for linear material behaviour and under the assumption that the damage is localized and affects the minority of the sensors; otherwise the damage information would alter the normalizing factor. In addition, it is important that the sensors contributing to the average value are all measuring homogeneous quantities (all measuring strain in the same direction as the normalized sensor and simultaneously), and this is guaranteed if the sensors are placed on stringers [32].

Damage indices are obtained for each sensor and for both the numerical and experimental data through the application of the scaling and normalizing procedures, as follows:

$$DI_k = \frac{\varepsilon_k \cdot SF_k}{\sum_{i=1}^{N} \varepsilon_i \cdot SF_i / N} \tag{1}$$

ε_k is the strain measured at the k^{th} sensor, SF_k is the scaling factor associated to the k^{th} sensor and used to calibrate its measure on the baseline numerical model, N is the number of strain gauges belonging to the network. The validation errors are reported in the right column of Table IV. This error is associated to the damage model and to non-normalized time variable influences (as those occurring if temperature affects each sensor to a different extent), referring to the same damage configuration considered previously.

Damage index sensitivity as a function of crack length is clearly visible in Figure 13, calculated when a constant 35 kN load was applied. In particular, Figure 13(c) shows the damage index evaluated for the sensor highlighted in Figure 13(a) during test 1–4, with a propagating skin crack. Because of the scaling procedure, numerical and experimental damage indices overlap in healthy condition, while their discrepancy increases with the damage dimension. However, the numerical information corresponds with the effective experimental sensitivity. The same damage index curve is shown in Figure 13(d) for the two sensors identified in Figure 13(b), with skin crack propagating after stringer failure (Test 5). The failed stringer loses a big portion of its load transfer capability, which is reflected in a steep decrease of the strain measured by sensor ID13. In a typical damage tolerant scenario, adjacent stringers must carry additional load, provoking the strain increase measured by sensor ID8. Again, the numerical reproduction of the experimental scenario is able to describe with certain accuracy the occurring phenomenon. This feature can thus be exploited for SHM purposes, especially for damage identification, as previously tested [5] by the authors during one fatigue crack propagation. Nevertheless, this is outside the aim of this paper, which is more focused on feature extraction and quantification of damage sensitivity during repeated fatigue crack propagation tests.

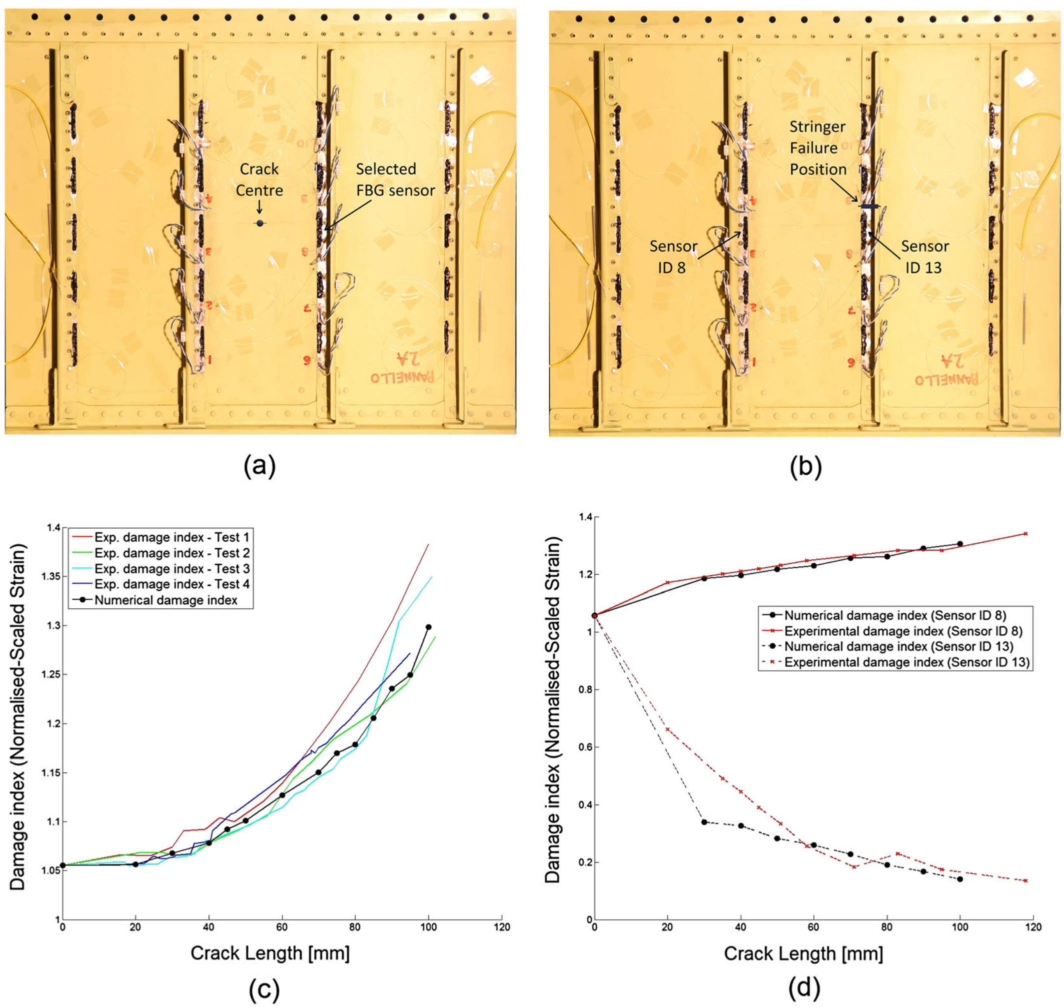

Figure 13. Damage index sensitivity as a function of crack length; comparison of numerical and experimental damage indices is shown in (c) and (d) for the sensor-damage configurations in (a) and (b), respectively.

7.4. Sensitivity to external load

The experimental and numerical damage index curves reported in Figure 13(c) and (d) have been calculated always referring to one static load condition (35 kN), to better appreciate the damage sensitivity of the selected feature (Eqn (1)). As anticipated in the preceding text, the best damage index for SHM design would maximize damage sensitivity, however reducing to a minimum the dependence on operative conditions, mainly load and temperature. Load sensitivity is clearly highlighted in Figure 14(a)–(d), for the

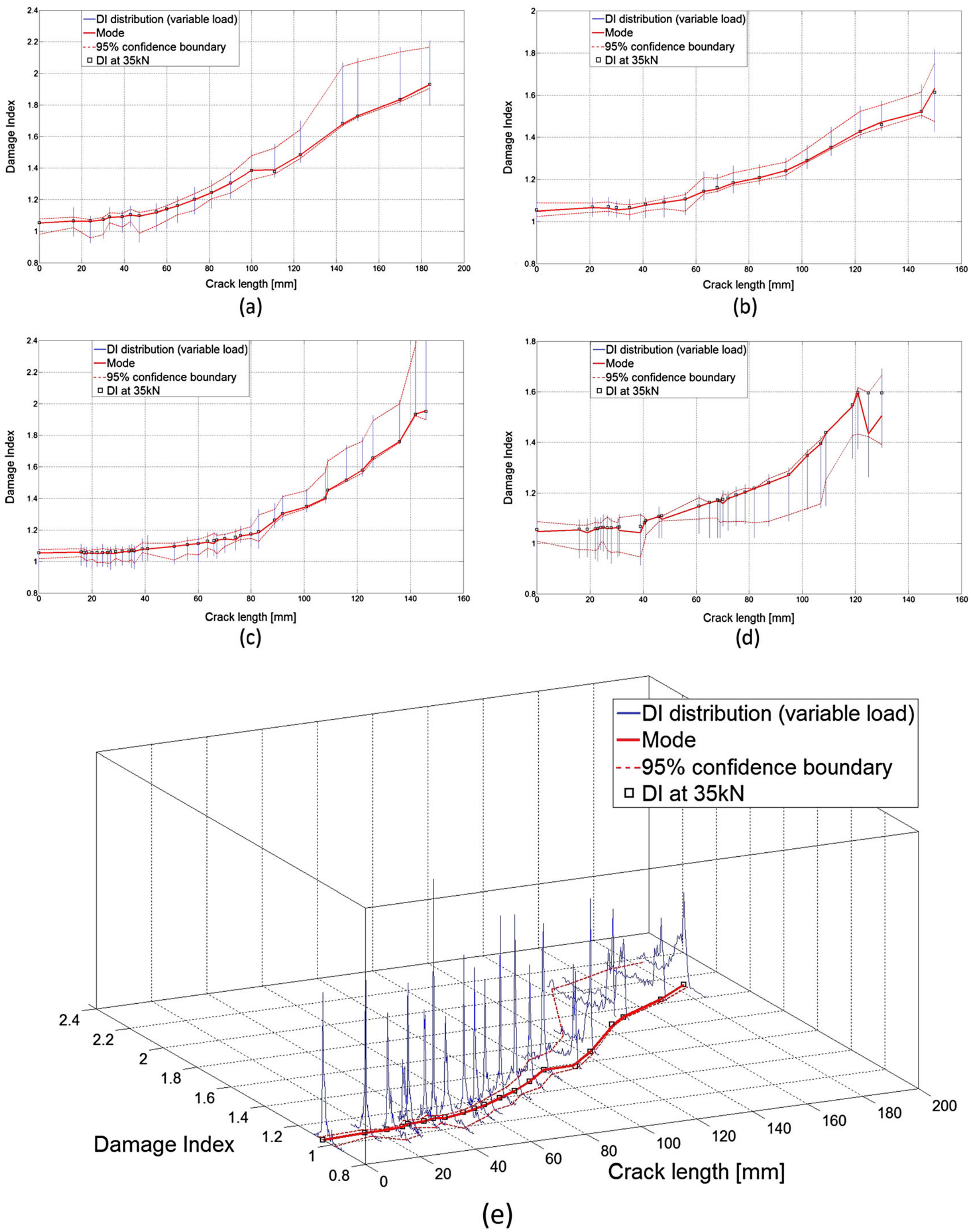

Figure 14. Random variable load effect on damage index curves, calculated during tests (a) 1, (b) 2, (c) 3, (d) 4 and (e) 3D representation of damage index distributions due to variable load during test 1.

tests 1–4, respectively. In particular, 1000 damage indices have been calculated at each crack length level, randomly selecting the load level from a uniform distribution with limits 3.5 and 35 kN, thus obtaining the damage index distributions reported in Figure 14, specifically for the sensor identified in Figure 13(a). The modes as well as the 2.5 and 97.5 percentile curves have been indicated for each test and at each crack length level. The damage indices calculated at constant 35 kN load have also been indicated as a term of comparison. Given the linearity of the numerical problem, FEM results have not been included here. On the other hand, a consistent amount of non-linearity was found analysing experimental data. It is related to non-linear load transfer from the structure to the sensor, sensor noise and non-homogeneous temperature influences (especially during test case 4, when the temperature was not compensated). It is also reasonable to expect the growth of non-linear effects for longer cracks. As a matter of fact, this is reflected in the enlargement of damage index distributions during crack propagation. Nevertheless, considering the tri-dimensional representation of damage index distributions in Figure 14(e), it is clear that most of the said uncertainties could be filtered out allowing multiple measures, then taking the mode of the resulting damage index distribution as reference, however, under the hypothesis of uniformly distributed loads.

Finally, based on data reported in Figure 14 for tests 1–4, the width of the 95% confidence range for the damage index calculated in baseline condition is about 25% the damage index sensitivity for a 100 mm crack damage. It has to be stressed that the indicated percentage is valid for the specific case under consideration, in terms of applied load range as well as sensor, damage and specimen geometry configurations (sensor and damage as in Figure 13(c)). Nevertheless, it allows to quantitatively appreciate the extent of load influence over the selected feature.

7.5. Suitability for on-board monitoring

HBM OptiMet-OMF bare optical fibre with Ormocer coating has been used. FBG sensors have been inscribed into the fibre. The installation of such sensors is quite complex, due to the fragility of the fibre when bent and the requirement of a certain amount of pre-straining during the glueing process. Even though pre-strained FBG sensors are sold by the majority of manufacturers, the physical dimension of the sensor is often too large for some applications, like for the fuselage panel under examination (due to the limited space available on stringers).

Removal of the primer coating is required for a perfect adhesion to the monitored structure. Nevertheless, the durability and the fatigue resistance of the sensor are very high. No sensor failures have been registered during a test programme that involved the utilization of 100 FBGs for crack propagation monitoring (the average duration of the tests was 400 000 cycles with an average strain peak level of 700 $\mu\varepsilon$).

Even though the sensitivity to damage is good, the main problem of using strain related features for SHM is that strain is sensitive to both the damage and the boundary conditions, primarily load. It is thus very important to properly normalize each sensor to highlight damage sensitivity only. Furthermore, any SHM system based on strain field modification is only suitable for online maintenance, unless residual stresses are addressed.

Another drawback of FBG technology is the high temperature sensitivity (temperature influences the mechanical strain as well as the refraction index of the sensor), and the helicopter is usually certified for a very wide range of temperatures, ranging from −40 °C to +50 °C. Even though temperature compensators are available, the robustness of the entire sensor network has to be carefully analysed.

Furthermore, as anticipated in Section 7.2, Bragg grating position inside the optical fibre is usually statistically determined (Figure 12). Though one might exploit temperature sensitivity to identify more precisely the sensor position inside the optical fibre, this is a drawback with respect to metal foil strain gauges, especially if one has to compare numerical and experimental data for components with high stress gradients. Another limitation might arise if a very close spacing between consecutive FBG sensors is required. In practice, both the technological process for FBG chain manufacturing and the signal processing algorithms for the identification of the FBG reflected spectra impose a minimum distance between two consecutive sensors that has to be accounted for during sensor network design. Good practice suggests providing at least 2.5 cm distance between two FBG centres for a 5 nm spectral span.

Nevertheless, FBGs do not require calibration (differently from metal foil strain gauges) and allow for sensor multiplexing. In practice, even though only five Bragg gratings per channel have been acquired during the tests (with a four-channel optical interrogator), the number of multiplexed sensors can be much increased. This number is however limited by the maximum level of strain that has to be measured. This will drastically reduce the amount of cables for the signal transmission with respect to SGs.

Finally, like CVM systems, FBGs are non-electrical sensors, suitable to any environment where EMI is a safety issue, e.g. for aeronautical applications.

8. PIEZOELECTRIC SMART LAYER

Two helicopter fuselage panels have been tested with a piezoelectric SL (refer to tests 6 and 7 in Table II). Twenty-four piezoelectric transducers were embedded into the SL film and applied to the structure as indicated in Figure 16(a) and (d) to diagnose skin crack (Figure 2(a)) and stringer failure (Figure 2(b)) damages, respectively. Damage-dependent feature extraction and damage sensitivity analysis based on signal cross-correlation coefficient are presented in Section 8.1, where the attention is focused on some selected paths, as indicated in Figure 16(b) and (e). Feature extraction is based hereafter on baseline comparison and any mismatch with respect to baseline condition might be seen as a perturbation while interpreting damage indices. The quantification of the effect of load variation over Lamb wave signals has been addressed in Section 8.2. The global evaluation of the structural health condition is performed in Section 8.3, based on ACESS software, developed by *Acellent Technologies Inc*. and suited to process SL data.

8.1. Feature extraction and sensitivity to damage

The paths indicated in Figure 16(b) and (e) have been selected to show Lamb wave signal sensitivity to damage. *Path 1* travels across the skin crack located in the centre of the panel bay (Figure 2(a)). *Path 2* travels across the crack initiated after stringer failure (Figure 2(b)). The actuator is excited at a frequency (150 Hz) that guarantees the presence of only the two fundamental Lamb wave propagation modes (symmetric and anti-symmetric), at least before any reflection is induced by geometric boundaries or by the damage itself. The signal dependence on crack length can be appreciated in Figure 15(a). The focus is on a particular time window where the first wave packets for the symmetric and anti-symmetric modes appear on the left and right sides, respectively. In general, the presence of crack damage along the actuator-sensor path induces a delay as well as signal peak reduction.

Among the various indices available in literature to extract damage-dependent features from Lamb wave signals [37], the cross-correlation has been selected here as a means to evaluate the correlation of a time signal ($y(t)$, relative to any possible damaged case) with the baseline signal ($b(t)$, relative to the undamaged situation). The cross-correlation $R_{by}(d)$, as a function of the delay d between the two signals can be expressed as,

$$R_{by}(d) = \frac{\sum_i \left[\left(y(i) - \mu_y\right)(b(i-d) - \mu_b)\right]}{\sqrt{\sum_i \left(y(i) - \mu_y\right)^2} \sqrt{\sum_i (b(i-d) - \mu_b)^2}} \tag{2}$$

μ_y and μ_b are the mean of the $y(t)$ and $b(t)$ signals, respectively, i is an index referring to the i^{th} sample of the signals and $R_{by}(d)$ is a vector indicating the correlation of the two signals as a function of the imposed delay d. The cross-correlation vector is reported in Figure 15(b) for different crack length levels and is calculated with respect to the baseline condition (0 mm crack).

Furthermore, the peak of the cross-correlation vector has been normalized with respect to the peak of the autocorrelation functions calculated on the baseline and damaged signal, thus obtaining a normalized cross-correlation coefficient (often referred to as local coherence [37]) according to the following procedure:

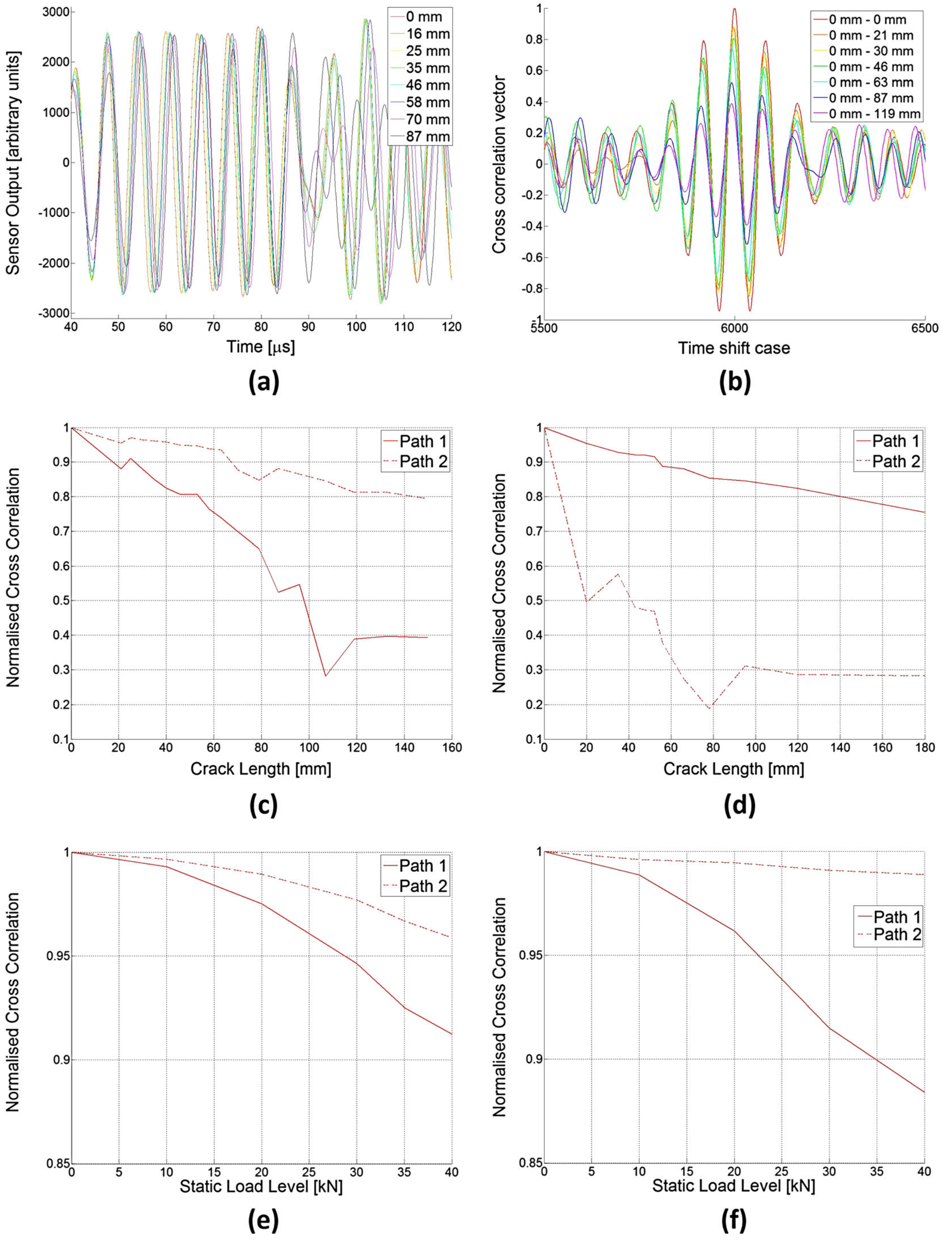

Figure 15. Lamb wave signal sensitivity to damage and load. (a) Time signals recorded for different skin crack length and relative to the path shown in Figure 15(b), and (b) cross-correlation vectors calculated for different skin crack lengths with respect to the baseline condition. (c) Damage index as a function of skin crack length and relative to the paths indicated in Figure 15(b). (d) Damage index as a function of skin crack length after stringer failure and relative to the paths indicated in Figure 15(e). (e) Load effect over damage index for the paths indicated in Figure 15(b) and (f) load effect over damage index for the paths highlighted in Figure 15(e).

1. Calculate the cross-correlation function between any signal in the presence of a damage and the related baseline signal, thus obtaining the cross-correlation vector $R_{by}(d)$.
2. Extract the peak value of the cross-correlation function for each available damage case.

3. Calculate the autocorrelation functions relative to the baseline $R_{bb}(d)$ and damaged $R_{yy}(d)$ signals, thus obtaining the autocorrelation vectors as follows:

$$R_{bb}(d)=\frac{\sum_i[(b(i)-\mu_b)(b(i-d)-\mu_b)]}{\sqrt{\sum_i(b(i)-\mu_b)^2}\sqrt{\sum_i(b(i-d)-\mu_b)^2}};R_{yy}(d)=\frac{\sum_i\left[\left(y(i)-\mu_y\right)\left(y(i-d)-\mu_y\right)\right]}{\sqrt{\sum_i\left(y(i-d)-\mu_y\right)^2}\sqrt{\sum_i\left(y(i-d)-\mu_y\right)^2}} \tag{3}$$

4. Extract the peak values of the autocorrelation functions, corresponding to the solution at zero lag (d = 0).
5. Normalize the cross-correlation peak value obtained at step (2) by the autocorrelation peak values calculated at step (4) to obtain the damage index (*DI*) associated to the k^{th} path, as follows:

$$DI_k=\frac{\max_d\left(R_{by}(d)\right)}{\sqrt{R_{bb}(0)\cdot R_{yy}(0)}} \tag{4}$$

The damage index sensitivity as a function of skin crack length (test 6) can be appreciated in Figure 15(c). A trend can be clearly identified for *path 1*, which passes across the crack. Much lower sensitivity has been found analysing the signals relative to *path 2*. Nevertheless, some disturbances are also evidently present. These are expected to be related to mismatched environmental and operational conditions, load in particular. Mismatch is intended between the actual signal and the baseline recorded signal. In practice, sensor signals have been acquired in real-time during fatigue crack propagation, while a sinusoidal 12Hz load was applied, with a peak load of 35kN and a load ratio of 0.1. Even though the test dynamics are by far slower than the Lamb wave dispersion, there is no control on the load level during the Lamb wave signal acquisition. This can induce two primary effects [38]: (1) specimen dimension (and in part also contact geometries) changes and (2) guided wave speed changes due to the acoustoelastic effect. Both of these changes perturb the time of arrival of individual echoes. Though it is not the major problem here (load ratio 0.1), variable load might also induce crack closure, thus significantly changing the signal transmission across the damage.

Similar considerations are valid for Figure 15(d), where the same damage index has been calculated for a crack propagating after stringer failure (Test 7) and relatively to the two paths indicated in Figure 16(e). The damage index relative to *path 1* (the same used before for the analysis of Test 6) presents a clear decreasing trend; nevertheless a smaller sensitivity has been found (compared to Figure 15(c)), being the damage not centred with respect to the path. Considering *path 2*, a steep decrease of the associated damage index is obtained after the artificial induction of stringer failure and crack initiation, while the damage index sensitivity decreases during fatigue crack propagation.

8.2. Sensitivity to external load

The same correlation index reported in Eqn (4) has been used to investigate the correlation of two signals acquired with different applied external loads. Given the fatigue load adopted during fatigue crack propagation tests was ranging between 3.5kN and 35kN, Lamb wave signal sensitivity to load has been verified in the 0-40kN range. In particular, no damage is introduced and different levels of static load have been applied [0, 10, 20, 30, 40kN]. The same static load test has been repeated on two different panels (tests 6 and7, before crack initiation and propagation), and the correlation indices have been calculated for the actuator-sensor paths indicated in Figure 16(b,e). Results have been reported in Figure 15(e) and (f).

A well definite trend can be observed in damage index variation as a function of load. It is clear that different paths experience different amounts of load sensitivity. In particular, *path 1* appears to be more sensitive to the applied load than *path 2*. This is probably due to different locations over the structure being exposed to different stress and strain levels. As an example, the uncertainty attributable to load variation over the damage index is in the order of 10% for *path 1* and below 5% for *path 2*. This has to be taken into consideration while attributing a confidence to the curves identified in Figure 15(c) and (d).

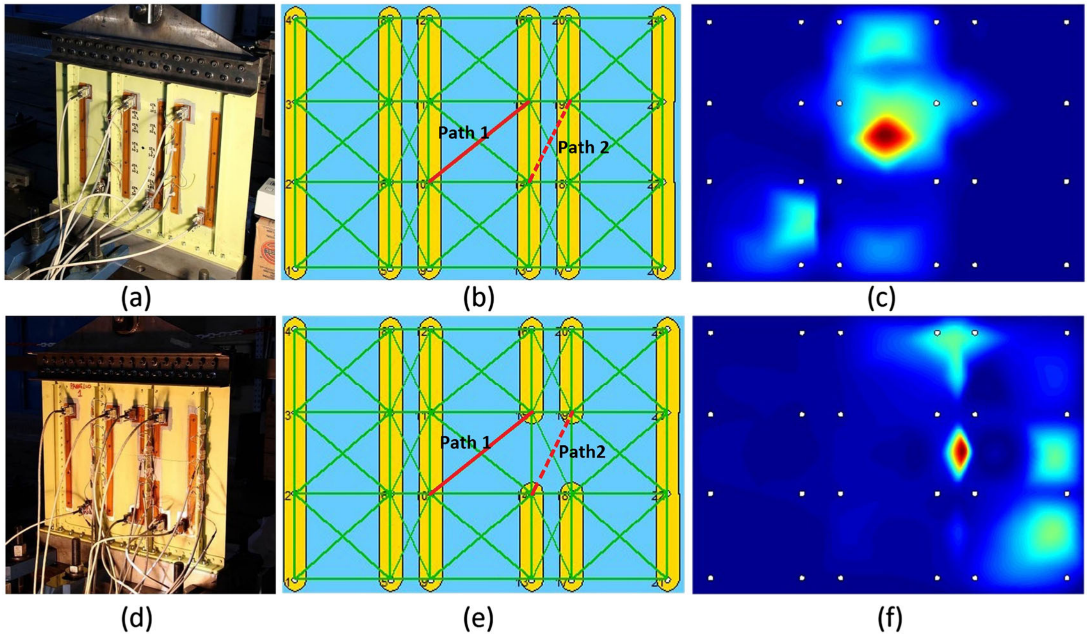

Figure 16. Diagnosis with a piezoelectric Smart Layer through ACESS software. The test rig, the overall selected actuator-sensor signal paths and the diagnostic results are presented in (a), (b) and (c), respectively, for the skin crack damage and in (d), (e) and (f), respectively, for the stringer failure damage.

Finally, based on data reported in Figure 15(c) and (e), the damage index variation due to load modification (calculated in baseline condition) is about 15% the damage index sensitivity for a 100 mm crack damage. It has to be stressed that the indicated percentage is valid for one specific path (path 1) and for the load range, sensor network, damage and specimen geometry configurations under analysis (Figure 16(a)). Nevertheless, it allows to quantitatively appreciate the extent of load influence over the selected feature.

8.3. Damage diagnosis with ACESS software

Two full diagnostic tests have been executed on two aluminium panels, where a skin crack damage and a stringer failure were, respectively, induced. Each actuator communicates with its neighbouring sensor, and a total number of 136 paths have been scanned in real-time at different levels of crack length during fatigue crack propagation, as indicated in Figure 16(b) and (e). Signals are then processed through ACESS software, where the following post-processing procedure has been selected among those available:

1. The residual signal (often referred to scatter signal) which is assumed to arise from damage is obtained by subtracting baseline signals recorded from the damage-free structure from real-time test signals.
2. The total strain energy (summation of the square of the scatter signal) is evaluated for each available path.
3. The damage index is compared with a threshold to provide the colour maps indicated in Figure 16.

Results are reported in Figure 16(c) where the diagnostic image is calculated for a 55 mm skin crack located in the centre of the panel bay. Figure 16(f) refers to the case when artificial stringer failure is induced, with 20 mm skin crack. In both cases, damage has been correctly identified and localized.

8.4. Suitability for on-board monitoring

Compared with FBG system technology, a piezoelectric sensor network involves the installation of many electrical circuits to power and to acquire the signal from each transducer. Moreover, it might induce EMI with the currently installed hardware. On the other hand, the SL sensor network proved

Table V. Comparison between fibre Bragg grating and Smart Layer sensor networks.

	Strain field (FBG)	Lamb wave scatter (SL)
Signal type	Non-electrical	Electrical
Installation	Experience required (Bare fibre)	Easy (SL)
Impact (logistic)	Low–Medium	Medium (SL)
Primer removal	Required	Required
Offline application	Not affordable	Some issues due to crack closure
Online application	Affordable	Affordable
Damage index sensitivity	Medium	Moderate
Suitability for large areas	Moderate	Moderate
Suitability for anomaly detection	Medium	Moderate
Suitability for localization	Moderate	Moderate
Suitability for damage description	Medium	Low
Required experience for damage description	Yes	Yes
Sensitivity to operational environment	High	Medium

FBG, fibre Bragg grating; SL, Smart Layer.

to be easy to install as it fully eliminates the need for each sensor to be installed and individually cabled. Nevertheless, the manufacturer suggested removing the primer coating to ensure perfect adhesion of the piezoelectric transducers with the monitored fuselage panel. In fact, the presence of coating may affect the Lamb wave transmission, which can be an issue especially in case of comparison between the experimental signal and any numerical or analytical solution.

Though Lamb waves still consist in mechanical strain waves, one advantage with respect to strain field-based systems is that Lamb wave approach involves very high frequencies (several applications range from 50 kHz to 300 kHz) and very high wave propagation velocities,[‡] thus being much less sensitive to boundary manoeuvre loads, typically characterized by low frequency and high amplitudes. However, any deformation might slightly change the specimen geometry as well as the wave propagation velocity, thus affecting the damage inference process too. Furthermore, one has to consider high frequency load spectrum induced by rotor dynamics, then choosing an actuation signal frequency sufficiently distant. If piezoelectric transducers are adopted in SHM, one has to carefully consider the effect of environmental and operational conditions, especially if baseline comparison approach is adopted. Temperature, load, surface wetting, etc. are all parameters to be addressed as they can potentially change with respect to the baseline condition, thus provoking misclassifications in the structural health condition estimate. The Lamb wave scatter sensitivity might be exploited for SHM both online and offline. Nevertheless, crack closure after load removal has to be addressed as it can induce significant changes in the signal transmissibility across the damage.

Focussing on the Lamb wave signal processing, additional complexity (with respect to strain field signal processing) is connected with the selection of the most suitable time window containing the most accurate information about damage. In practice, this is a non-trivial aspect as a Lamb wave signal contains different wave packets associated to different propagating modes as well as to boundary and damage reflections. If a precise damage index trend is desired, one has to carefully select the time domain for the signal processing.

Concerning SL in particular, which is based on a pure data-driven approach, to date the system appears to be good for the detection and localization of damage. Nevertheless, it fails to provide an indication of the damage type and quantification assessment, which are two major parameters required to perform prognosis. It also requires the definition of a threshold, not easily accessible a priori with respect to experimental activity. As a matter of fact, one must have information on the extent of external influences on the baseline condition (like reported in Section 8.2 specifically for the load effect) in order to set a decision boundary for anomaly detection. No sensor de-bonding has been encountered during the fatigue tests, nevertheless, the electrical circuits embedded into the SL film broke after the passage of the skin crack during test 6.

A comparison summary between FBG and SL sensor networks is reported in Table V.

[‡]The group velocity has been estimated from dispersion curves as 5402 and 2025 m/s for the anti-symmetric and symmetric fundamental modes, with a 0.81 mm skin thickness and 150 kHz tone-burst frequency.

9. CONCLUSIONS

Many different sensor technologies are available nowadays, some of them being currently used for aircraft scheduled maintenance [2]. Some selected sensor technologies have been applied in this work to monitor fatigue crack damage on a typical aeronautical panel, constituted of a skin stiffened through some riveted stringers, and specific conclusions have been provided throughout the document concerning their suitability for SHM. Reported results refer to a test programme where seven fatigue crack propagations have been performed on the same structure geometry with different sensors installed. Local sensors (ECGs and CVM) and a distributed sensor network (based on optical FBG and piezoelectric transducers) have been considered in this paper. A transversal classification has been established between electrical sensors (ECGs and piezoelectric transducer network) and non-electrical sensors (CVM and FBG sensor network). Furthermore, metal foil SGs have also been installed to verify the optical gauge signal. The aim is to appreciate and compare the extent of the damage-related feature sensitivity as well as to share the results and the practical experience gained trying to address on-board real-time feature extraction. In practice, it is impossible to identify a priori the best sensor technology for crack diagnosis as it strongly depends upon the geometry and material of the monitored component, the operational environment (including but not limited to load and temperature variation), the target damage to be identified, cost-benefit trade-off analyses, etc.

If local monitoring is desired, crack gauges are a valid possibility. Even though CVM is particularly sensitive to crack closure if used offline, it proved to be effective for on-board application. CVM consists of on/off sensors providing direct indication of occurring damage and can also be designed to monitor relatively large areas. If used locally, experience is needed to correctly estimate the position where a crack is likely to nucleate, and this experience is potentially retrieved from on-the-field activity, experimental tests or numerical models.

In some cases, the presence of many nucleation points (such as rivet holes in airframe structures) makes the identification of hot spot regions a non-trivial task. In practice, the probability of crack nucleation can be equally distributed on a relatively large region. One might resort to distributed sensor networks. The main issue related to such systems is that they do not measure damage, but provide a signal (in general one signal from each sensor) from which a damage dependant feature has to be extracted (damage index). The influence of environmental and operational varying conditions is a crucial aspect to be addressed. In fact, strain field sensitivity to damage (based on FBG technology) and Lamb wave scatter dependence on damage (based on piezoelectric transducer network) have been investigated. In both cases, feature extraction involved the comparison with a baseline condition. In the best case scenario, every departure from the baseline condition can be associated to the occurring damage. Nevertheless, any mismatch with respect to external loads, temperature, surface condition, etc. will provoke a modification on the baseline reference condition (healthy structure) that has to be accounted for in order to provide a robust sensitivity curve. The effect of load variation on the selected damage indices has been quantified inside this work, specifically concerning the distributed network technologies (FBG and SL).

A further comment has to be made concerning the level of the SHM system to be provided. If only the triggering of an alarm is required, any on/off sensor might be sufficient for that scope, and CVM is a valid technology if relatively large areas are concerned. If an electrical crack gauge is adopted, one might obtain an indication on damage propagation too, given the crack passes through the sensor. In general, if damage assessment is required (in terms of position, dimension and type), one has to select a feature that is dependent on those damage parameters. Strain field and Lamb wave scatter are two possibilities, each one requiring the design of a damage index suitable for robust feature extraction from signals. An additional problem arises. In fact, one always needs to interpret the feature extracted from a sensor network in order to provide damage description. On the one hand, it is possible to declare an alarm and to localize a damage based on actual signal comparison with a baseline condition, given the influence of environmental and operational conditions is addressed. On the other hand, if the complete damage assessment problem is required, one would need information relative to the structures with all conceivable damage locations and severities for example. It has been shown as part of the present research that numerical models can be used to retrieve this information. However, they require the design of a proper validation test programme to appreciate the uncertainty related to the modelled phenomenon.

REFERENCES

1. Broek D. *Elementary Engineering Fracture Mechanics*. Kluwer Academic Pub, Dordrecht, the Netherlands, 1986.
2. Staszewski W, Boller C, Tomlinson G. *Health Monitoring of Aerospace Structures: Smart Sensor Technologies and Signal Processing*. John Wiley & Sons Ltd, Chichester, England, 2004.
3. Department of USA defence. Joint Service Specification Guide – Aircraft Structures (JSSG-2006).
4. Sbarufatti C, Manes A, Giglio M. Sensor network optimization for damage detection on aluminum stiffened helicopter panels. *Proc. Coupled Problems* 2011: 1107–1119.
5. Sbarufatti C, Manes A, Giglio M. Performance optimization of a diagnostic system based upon a simulated strain field for fatigue damage characterization. *Mechanical Systems and Signal Processing* 2013; **40**:667–690.
6. Farrar CR, Park G, Allen DW, Todd MD. Sensor network paradigms for structural health monitoring. *Structural Control and Health Monitoring* 2006; **13**:210–225.
7. http://www.hbm.com/en/menu/products/strain-gages-accessories/strain-gauges-for-stress-analysis/rds/
8. http://www.smsystems.com.au/
9. Roach D. Real time crack detection using mountable comparative vacuum monitoring sensors. *Smart Structures and Systems* 2009; **5**(4):317–328.
10. Kollgaard WG, Register J, Zaidi M. Comparative vacuum monitoring (CVM™) as an alternate means of compliance (AMOC). *Insight* 2005; **47**(3):153–156.
11. Worden K, Manson G, Allman D. Experimental validation of a structural health monitoring methodology: part I. Novelty detection on a laboratory structure. *Journal of Sound and Vibration* 2003; **259**(2):323–343.
12. Manson G, Worden K, Allman D. Experimental validation of a structural health monitoring methodology: part II. Novelty detection on a gnat aircraft. *Journal of Sound and Vibration* 2003; **259**(2):345–363.
13. Manson G, Worden K, Allman D. Experimental validation of a structural health monitoring methodology: part III. Novelty detection on an aircraft wing. *Journal of Sound and Vibration* 2003; **259**(2):365–385.
14. Kraft M, White NM. *MEMS for Automotive and Aerospace Applications*. Woodhead Publishing, Cambridge, England, 2013.
15. Hui J, Xiaopeng W, Meiying Z. Composite skin/stringer panel damage detection based on modal strain energy and neural network technique. *Applied Mechanics and Materials* 2011; **66**:322–327.
16. Sahin M, Shenoi RA. Quantification and localization of damage in beam-like structures by using artificial neural networks with experimental validation. *Engineering Structures* 2003; **25**:1785–1802.
17. Giglio M, Manes A. Crack propagation on helicopter panel: experimental test and analysis. *Engineering Fracture Mechanics* 2008; **75**:866–879.
18. Giglio M, Manes A, Fossati M, Mariani U, Giani C. Comparison of fatigue crack propagation behavior of Al 2024 and Al–Li 8090 helicopter fuselage panels. *Journal of Testing and Evaluation* 2009; **38**(1):73–82.
19. Katsikeros CE, Labeas GN. Development and validation of a strain-based structural health monitoring system. *Mechanical Systems and Signal Processing* 2009; **23**(2):372–383.
20. Lin M, Chang FK. Development of smart layer for built-in diagnostics for composite structures. *Proc. 13th Technical Conference of the American Society for Composites*, Baltimore, 1998.
21. Ihn JB, Chang FK. Detection and monitoring of hidden fatigue crack growth using a built-in piezoelectric sensor/actuator network: I. Diagnostics. *Smart Materials and Structures* 2004; **13**:609–620.
22. Lee BC, Staszewski WJ. Modelling of lamb waves for damage detection in metallic structures: Part I. Wave propagation. *Smart Materials and Structures* 2003; **12**:804–814.
23. Park G, Farrar CR, di Scalea FL, Coccia S. Performance assessment and validation of piezoelectric active-sensors in structural health monitoring. *Smart Materials and Structures* 2006; **15**:1673–1683.
24. Viktorov IA. *Rayleigh and Lamb Waves - Basic Principles*. Plenum: New York, 1967.
25. Rose JL. *Ultrasonic Waves in Solid Media*. Cambridge University Press: Cambridge, 1999.
26. Su Z, Ye L. Lamb wave propagation-based damage identification for quasi-isotropic CF/EP composite laminates using artificial neural algorithm: part I – Methodology and database development. *Journal of Intelligent Material Systems and Structures* 2005; **16**:97–111.
27. Su Z, Ye L. Lamb wave propagation-based damage identification for quasi-isotropic CF/EP composite laminates using artificial neural algorithm: part II – Implementation and validation. *Journal of Intelligent Material Systems and Structures* 2005; **16**:113–125.
28. Sbarufatti C, Manson G, Worden K. A numerically enhanced machine learning approach to damage diagnosis using a lamb wave sensing network. *Journal of Sound and Vibration*, review pending.
29. http://www.saristu.eu/
30. http://www.acellentsensors.com/
31. Colombo D, Giglio M, Manes A. 3D fatigue crack propagation analysis of a helicopter component. *International Journal of Materials and Product Technology* 2007; **30**:107–123.
32. Sbarufatti C, Manes A, Giglio M. Probability of detection and false alarms for metallic aerospace panel health monitoring. *Proc. 7th Int. Conf. on CM and MFPT* 2010.
33. CVM™ Laboratory System Manual. Structural monitoring systems, April 2006, Issue 6.
34. Swift T. Damage tolerant analysis of redundant structures. Douglas Aircraft Company, Mc Donnell Douglas Corporation, AGARD lecture series 97, Fracture Mechanics Design Methodology 1979.
35. Kreuzer M. *Strain Measurement with Fiber Bragg Grating Sensors*. HBM: Darmstadt, Germany.
36. http://www.hbm.com/en/menu/products/strain-gages-accessories/optical-strain-gauges/optimet
37. Michaels JE. Detection, localization and characterization of damage in plates with an *in situ* array of spatially distributed ultrasonic sensors. *Smart Materials and Structures* 2008; **17**:035035.
38. Chen X, Michaels JE, Lee SJ, Michaels TE. Load-differential imaging for detection and localization of fatigue cracks using Lamb waves. *NDT&E International* 2012; **51**:142–149.